



Published in final edited form as:

Nat Commun. 2013 ; 4: 1739. doi:10.1038/ncomms2772.

Dynamic Self-Stiffening in Liquid Crystal Elastomers

Aditya Agrawal¹, Alin C. Chipara², Yousif Shamoo³, Prabir K. Patra⁴, Brent J. Carey², Pulickel M. Ajayan², Walter G. Chapman¹, and Rafael Verduzco¹

Rafael Verduzco: rafaelv@rice.edu

¹Department of Chemical and Biomolecular Engineering, Rice University, MS-362, 6100 Main Street, Houston, TX 77005 (USA)

²Department of Mechanical Engineering and Materials Science, 6100 Main Street, Rice University, MS-321, Houston, TX 77005 (USA)

³Department of Biochemistry and Cell Biology, 6100 Main Street, Rice University, MS-140, Houston, TX 77005 (USA)

⁴Departments of Biomedical Engineering and Mechanical Engineering, 126 Park Avenue, University of Bridgeport, Bridgeport, CT 06604 (USA)

Abstract

Biological tissues have the remarkable ability to remodel and repair in response to disease, injury, and mechanical stresses. Synthetic materials lack the complexity of biological tissues, and man-made materials which respond to external stresses through a permanent increase in stiffness are uncommon. Here, we report that polydomain nematic liquid crystal elastomers increase in stiffness by up to 90% when subjected to a low-amplitude (5%), repetitive (dynamic) compression. Elastomer stiffening is influenced by liquid crystal content, the presence of a nematic liquid crystal phase and the use of a dynamic as opposed to static deformation. Through rheological and X-ray diffraction measurements, stiffening can be attributed to a nematic director which rotates in response to dynamic compression. Stiffening under dynamic compression has not been previously observed in liquid crystal elastomers and may be useful for the development of self-healing materials or for the development of biocompatible, adaptive materials for tissue replacement.

Introduction

Biological tissues have the remarkable ability to remodel and repair in response to disease, injury, and mechanical stresses¹⁻³. Well-known examples include bone remodeling and

Users may view, print, copy, download and text and data- mine the content in such documents, for the purposes of academic research, subject always to the full Conditions of use: http://www.nature.com/authors/editorial_policies/license.html#terms

Correspondence to: Rafael Verduzco, rafaelv@rice.edu.

Author Contributions

AA and RV designed the experiments. AA and ACC performed the dynamic mechanical analysis experiments. AA performed the chemical synthesis, optical microscopy and 2DWAXD experiments. PMA provided the DMA Q800. YS provided the Rigaku Raxis-IV++. AA, PKP, PMA, WGC and RV analyzed the data. AA, BJC, PKP, PKA, WGC and RV wrote the manuscript.

Competing financial interests

The authors declare no competing financial interests.

strengthening through a process which involves changes in bone mass and porosity,⁴ and muscle development, tumor growth and blood vessel structure are all affected by mechanical stresses^{5–7}. Synthetic materials lack the complexity of biological tissues, and man-made materials which respond to external stresses through a permanent increase in stiffness are uncommon^{8,9}. Here, we report that polydomain nematic liquid crystal elastomers (LCEs) increase in stiffness by up to 90% when subjected to a low-amplitude (5%), repetitive (dynamic) compression. Such self-stiffening is uncharacteristic of synthetic rubbers^{9,10} but arises in polydomain LCEs due to the presence of a mobile nematic director that re-orientes in response to external stresses. The observed dynamic stiffening in polysiloxane LCEs may be useful for the development of self-healing materials and biocompatible, adaptive materials for tissue replacement. Additionally, the use of low-strain, repetitive compression represents a facile method to prepare uniformly aligned LCEs, which are typically prepared by applying large tensile strains or external fields during material synthesis^{11–16}. Previous work has focused on the properties of LCEs under large-strain deformation, but our findings indicate rich behavior at previously overlooked low-strain, dynamic deformations.

LCEs are comprised of a crosslinked network of flexible polymer chains with liquid crystalline order (Fig. 1a)^{17,18}. Polydomain LCEs were prepared by coupling liquid crystal mesogens to poly(hydrogenmethylsiloxane) (PHMS) (Fig. 1a), as has been previously reported.¹⁹ The resulting materials are rubbery ($T_g \approx -30$ °C), nematic networks with no global orientation of the nematic director (polydomain). Nematic order fundamentally alters the response of LCEs to external stresses. Network chains in LCEs are locally anisotropic and assume an ellipsoidal conformation, in contrast to the spherical random coil conformation of conventional isotropic rubbers. LCEs exhibit ‘soft elasticity’ which is exemplified by large-strain deformations with little resistance^{17,20,21}. Herein, we examine the behavior of polydomain LCEs under a repetitive, compressive deformation at low strains (5%). We find a significant increase in stiffness after extended compression and, through a combination of dynamic mechanical testing (DMA), 2-dimensional wide-angle X-ray diffraction (2DWAXD) and polarized optical microscopy (POM) can attribute microstructure changes to a mobile nematic director which re-orientes in response to dynamic stresses.

Results

Dynamic stiffening of polydomain LCEs

To investigate the role of mesogen content on mechanical properties, a systematic series of polydomain LCEs (LCE90, LCE80, LCE60, LCE40 and LCE20) were prepared with mesogen content ranging from 90 to 20 mol % relative to the Si-H bonds in the PHMS polymer (Table 1). Poly(dimethyl siloxane) (PDMS) was also studied for comparison to the LCEs. PDMS is chemically and mechanically similar to the LCEs studied, but with no mesogen content. Under 16 h of repetitive, compressive loading (5 Hz, 5 % strain), LCE90 exhibits a 90 % increase in stiffness (Fig. 1b). The strain amplitude is maintained at 5 % for the duration of the experiment. As shown in Table 1, the final stiffness of LCE90 surpasses the initial values of other LCEs studied despite the lower crosslink density of LCE90. Dynamic mechanical testing of all LCEs prepared shows that mesogen content is correlated

with increased stiffness, in particular for the series of samples where the crosslink density is held constant (LCE20, LCE40, and LCE60) (Fig. 2). LCE60 and LCE80 exhibit a similar, although less pronounced, stiffening response compared with LCE90. The stiffness increase under 5 % compressive loading is 63 % and 33 % for LCE80 and LCE60, respectively. LCE20 and LCE40, both with no nematic phase (Supplementary Figure S1), exhibit a stiffness increase of only 14%. Finally, PDMS exhibits a stiffness increase of only 1.4 %.

The presence of nematic order and the application of a repetitive (dynamic) load are essential to the stiffening response (Fig. 2). As shown in Fig. 2 (inset), LCE90 exhibits a modest increase in stiffness when dynamically compressed in the isotropic phase at 80 °C (~ 15 %, similar to LCE20 and LCE40) while stiffness increases by more than 80 % when the same measurement is carried out in the nematic phase at 45 °C. This same trend is observed for all nematic LCEs (see Supplementary Figure S2). Furthermore, stiffening is only observed under dynamic, compressive stress. An extended static compression test with an applied stress greater than the maximum stress applied during dynamic compression (70 kPa) and a strain of 6 % resulted in only a modest (~10 %) stiffness increase (see inset of Fig. 2 and Supplementary Figure S2). Thus, consistent with previous reports^{14,15}, a static deformation at low strain (<10 %) does not result in significant changes to the microstructure of the LCE. As an additional control experiment, samples held at 45 °C for at least 16 h in the DMA without compression show no stiffness increase.

LCE microstructure analysis

Microstructure changes in polydomain LCEs were analyzed by 2DWAXD before and after deformation. In the experimental configuration used for this study, scattering peaks corresponding to mesogen spacing along the molecular width are clearly resolved (Fig. 3), enabling quantification of orientational ordering of the mesogenic side-groups. X-ray scattering measurements were performed using a Rigaku Raxis-IV++ equipped with an incident beam monochromator, pinhole collimation (0.3 mm) and Cu X-ray tube ($\lambda = 1.54 \text{ \AA}$). The sample to detector distance was 100 mm. Before compressive deformation, all LCEs exhibit an isotropic scattering peak characteristic of a polydomain, nematic LCE (Fig. 3a). After dynamic compression, a clear anisotropy emerges in LCE90, LCE80, and LCE60 (see Fig. 3c). Anisotropic scattering is only observed in the x - z and y - z planes, but the scattering pattern in the x - y plane remains isotropic. This indicates that the nematic director in these samples rotates away from the z -axis (compressive direction) to lie primarily in the x - y plane but remains globally disordered in the x - y plane, resulting in an oblate LC orientation after dynamic compression. The reorientation of the LC side-groups can also be followed qualitatively through POM; global reorientation of the nematic director away from the z -axis is consistent with reduced light transmission through the x - z and y - z faces when crossed polarizers are aligned with the axis of compression (Fig. 3b).

Coupling between elastomer deformation and nematic director orientation

The dynamic mechanical analysis measurements together with WAXD patterns for stressed and unstressed LCEs establish a clear connection between stiffening and reorientation of the nematic LC director. In LCEs, network chain conformation is coupled to the nematic director orientation. Therefore, the observed re-orientation of the mesogenic side-groups

perpendicular to the compressive axis reflects a reorientation of the LCE network chains (Fig. 4c). The strain lines corresponding to a linear, compressive deformation can be calculated by performing finite element modeling (FEM) simulations using COMSOL Multiphysics 4.2 simulation package. Simulation results predict elongational strains in the plane perpendicular to the compressive axis. This elongational strain is expected to preferentially align the ellipsoidal LCE network chains in the x - y plane and, due to coupling between the LC side-group and polymer backbone, result in the observed reorientation of the nematic director. 2DWAXD images indicate reorientation of the LC side-groups in the x - y plane, consistent with a preferential orientation of the LC side-groups parallel to the polymer backbone. The 2DWAXD data also enable calculation of a macroscopic alignment

parameter $S = \langle \frac{3}{2} \cos^2 \theta - \frac{1}{2} \rangle$, averaged over the entire sample where θ is the angle between the local director orientation and the x - y plane^{22,23}. The increase in macroscopic alignment is directly correlated with mesogen content, as shown in Fig. 3d. Furthermore, the coupling between mesogen side-group orientation and polymer orientation results in macroscopic changes to sample dimensions. As shown in the Supplementary Table S1, dimensional changes up to 8.3% along compression (measure along z -axis) and 7.7% along x and y -axes are recorded, consistent with the coupling of macroscopic shape and global director orientation. Since the stiffening response arises due to a director reorientation, stiffening is fully reversible. This is demonstrated by the observed relaxation of a sample subjected to dynamic compression: after three months, the stiffness returns to its initial value and the director orientation is polydomain (Supplementary Figure S3). Similar relaxation is observed for a dynamically stressed sample annealed above the T_{NI} for 4 hours.

Discussion

The stiffening response can be understood within the theoretical framework of nematic rubber elasticity¹⁷. Warner et al. showed that for nematic LCEs, the free energy density satisfies the following equation: $F_{el} = \frac{1}{2} \mu \text{Tr} \left(\underline{\underline{l}} \cdot \underline{\underline{\lambda}}^T \cdot \underline{\underline{l}}^{-1} \cdot \underline{\underline{\lambda}} \right)$, where μ is the rubber elastic modulus, λ is strain and $\underline{\underline{l}}$ is the network step-length tensor that describes the local (generally anisotropic) chain conformation. This theory assumes Gaussian, phantom network chains and the absence of quenched disorder. A consequence of this free energy expression is that strains λ of the form $\lambda = \underline{\underline{l}}^{1/2} \cdot W_\alpha \cdot \underline{\underline{l}}^{-1/2}$, where W_α is an arbitrary rotation by an angle α , come with no increase to the elastic free energy. Thus, for this type of strain, the LCE deforms ‘softly’ with no resistance. This result only applies to the ideal case, but real elastomers more commonly exhibit semi-soft elasticity, with some resistance to deformation below a threshold stress value. An example of this for a polydomain LCE under uniaxial strain is shown in Fig. 4d; the elastomer exhibits, after a strain threshold, a pronounced plateau in the stress. This stress plateau is a direct result of ‘soft elasticity’ and is associated with nematic director rotations. At higher strains, the nematic director is fully aligned, and director reorientations can no longer accommodate further strain, resulting in a stress increase. This particular example reflects the behavior of LCEs under large (> 10%) uniaxial strains but similar behavior is observed in the present study for LCEs under compression. In initially unstressed samples, a ‘soft’ elastic response is observed. The softness or reduced

stiffness is a result of a globally disordered nematic director that can accommodate deformations through rotation. However, extended dynamic compression results in a reorientation of the nematic director and a corresponding increase in stiffness (Fig. 4d). Similar to the behavior of LCEs under uniaxial tension, reorientation of the nematic director is associated with an increased resistance to deformation.

A comparison of deformed and undeformed LCEs shows that the measured stiffness increase is a distinctly nonlinear phenomenon. As shown in Fig. 4d and the Supplementary Figure S3, there is no difference in stiffness between stressed and unstressed samples for strain values less than 1%. Thus, as expected, at low compressive strains LCEs behave linearly, and the slope of the stress-strain curve simply reflects the equilibrium Young's modulus. Differences between stressed and unstressed LCEs are only observed for strain values greater than approximately 2%. This threshold value may reflect "semi-softness" in LCEs which arises due to polymer chain length polydispersities, compositional fluctuations and other network non-idealities.

Strain-stiffening in LCEs contrasts with the irreversible softening of polymeric networks under cyclic strain, a phenomenon known as the Mullins effect^{9,10,24}. While the Mullins effect is not fully understood^{9,10}, it has been seen in crystallizable rubbers or rubbers with added fillers and has also been observed in biological tissue^{25,26}. Recently, stiffening behavior was reported for bundled actin networks under cyclic shear²⁷. This was observed at higher crosslink densities and attributed to the physical nature of the network, which allowed reorganization of the network constituents, resulting in hardening after cyclic shear²⁷. This contrasts with the dynamic stiffening reported here in covalent LCE networks. The novelty of the present work is the discovery of dynamic stiffening in a synthetic, homogeneous polymeric network with liquid crystalline order. Additionally, the presence of liquid crystal order enables quantitative characterization of side-group and network chain orientation before and after deformation, establishing a direct connection between stiffening and network chain conformation.

In summary, we report LCE self stiffening in response to dynamic, compressive loading. The stiffening behavior observed here is for a permanent network at low strains and can be attributed to a mobile nematic director. Director reorientation and alignment at low strains and dynamic compression has not been previously reported in LCEs and suggest underlying network relaxation modes at 5 Hz which govern the response. LCEs which increase in stiffness may be useful for the development of self-healing materials or for the development of biocompatible, adaptive materials for tissue replacement. Dynamic compression is a straightforward method for preparing uniformly aligned nematic LCEs, and may be applicable to higher-order liquid crystal phases, including chiral nematics and smectics. Other repetitive deformations (e.g. uniaxial tension, shear) at low strain values may lead to similar director reorientations in LCEs and will be the focus of future work.

Methods

Materials

Toluene, Pt-catalyst ((dichloro (1, 5-cyclooctadiene) platinum (II)), allylbromide, butanol, 11-bromo-1-undecene, sodium hydride (60% dispersion in mineral oil), hydroquinone, magnesium sulfate, PHMS (poly (hydromethylsiloxane)) ($M_w=1700-3200$ g/mole), ethyl acetate, 4-hydroxyl-4'-cyano biphenyl, sodium hydroxide, tetrahydrofuran (THF), diethyl ether, dimethyl formamide (DMF), 6-bromo-1-hexanol, benzene, methanol, and potassium carbonate were purchased from commercial suppliers and used as received. The crosslinker (1,4-di(10-undecenyloxy)benzene) was synthesized as described previously.²⁸ 4-(1-Hexanol oxy)-4'-cyano biphenyl and mesogenic side-group were prepared as described below (see Supplementary Figure S4 for reaction scheme).

Preparation of 4-(1-hexanol oxy)-4'-cyano biphenyl (3)

4-hydroxyl-4'-cyano biphenyl (1, 7mmol, 1.36g), 6-bromo-1-hexanol (2, 10mmol, 1.83 g), and K_2CO_3 (14mmol, 1.934g) were dissolved in 25 ml DMF and heated to 90 °C for 20 hours. The reaction was then quenched by adding water and filtering to collect a white precipitate. The precipitate was then dried under vacuum and recrystallized in benzene to obtain the desired product. 1H NMR (400 MHz, $CDCl_3$), δ (ppm): 7.8-7.6 (m, 4H) 7.54-7.50 (d, 2H), 7.0-6.9 (d, 2H), 4.20 (t, 2H), 3.36 (t, 2H), 1.8 (m, 2H), 1.7 (m, 2H), 1.40 (m, 4H).

Preparation of Mesogenic Side-Group (4)

3 (6 mmol, 1.77g) was slowly added to a solution of sodium hydride (12.5mmol, 0.3g) in 30 ml diethyl ether/ DMF (10:1). The reaction mixture was stirred under nitrogen atmosphere for 1 hour before cooling to 0 °C and adding a solution of allyl bromide (1.2 g, 10 mmol) in 5 ml diethyl ether dropwise. The reaction was allowed to proceed overnight before adding brine to quench the reaction. The layers were separated and the organic layer was washed with 1N HCl and water. The product was concentrated under reduced pressure and purified by column chromatography (silica gel, eluent: ethyl acetate/ hexanes 1:9 v/v). 1H NMR (400 MHz, $CDCl_3$), δ (ppm): 7.7-7.5 (m, 6H), 7.0-7.1 (d, 2H), 5.8 (m, 1H), 5.0 (d, 2H), 4.2 (t, 2H), 4.0 (d, 2H), 3.4 (t, 2H), 1.8-1.4 (m, 8H).

Preparation of polydomain LCE

Polydomain LCE samples were synthesized in the isotropic phase as described previously¹⁹. Briefly, mesogenic side-group (4), 4-(1-hexanol oxy)-4'-cyano biphenyl crosslinker and PHMS (poly (hydromethylsiloxane)) were dissolved in toluene along with the Pt catalyst, and the reaction was allowed to proceed for 70 °C for 3 days. Elastomers were then swollen in dichloromethane for several days to wash out the unreacted materials and nonreactive solvent. By gradually increasing the methanol content of swelling solvent, elastomers were deswollen and then air-dried before testing.

Dynamic Mechanical Analysis

For the DMA studies, the samples were razor cut to dimensions of 1.5 mm x 1.5 mm x 1 mm. All sample dimensions were measured using DMA and verified with a digital caliper.

Dynamic Mechanical Testing was carried out in compression mode as illustrated in Figure 1b using TA Instruments Q800 DMA at a 5% strain amplitude, 5 Hz frequency and at a preload of 0.01N. All the tests were conducted isothermally at 45°C, except where otherwise noted.

Supplementary Material

Refer to Web version on PubMed Central for supplementary material.

Acknowledgments

The authors like to thank Richard Crouse for assistance with 2DWAXD studies. The authors also acknowledge Shared Equipment Authority of Rice University for providing 2DWAXD instrumental facilities. This project was supported in part by the IBB Hamill Innovations Grant. R. Verduzco acknowledges support from the Robert A. Welch Foundation (Grant C-1750) and Louis and Peaches Owen. A. Agrawal and W. Chapman acknowledge financial support of the Robert A. Welch Foundation (Grant No. C-1241) and NSF CBET-0756166. Yousif Shamoo acknowledges support from NIH grant R01 AI AI080714 from the National Institute of Allergy and Infectious Diseases (NIAID).

References

1. Fung, YC. *Biomechanics: Mechanical Properties of Living Tissues*. 2. Springer; New York: 1993.
2. Jones GW, Chapman SJ. Modeling growth in biological materials. *Siam Rev.* 2012; 54:52–118.
3. Humphrey JD. Review Paper: Continuum biomechanics of soft biological tissues. *R Soc Lond Proc Ser A Math Phys Eng Sci.* 2003; 459:3–46.
4. Cowin, SC. *Bone Mechanics Handbook*. 2. CRC Press; Boca Raton: 2001.
5. Helmlinger G, Netti PA, Lichtenbeld HC, Melder RJ, Jain RK. Solid stress inhibits the growth of multicellular tumor spheroids. *Nat Biotechnol.* 1997; 15:778–783. [PubMed: 9255794]
6. Goldberg AL, Etlinger JD, Goldspink DF, Jablecki C. Mechanism of work-induced hypertrophy of skeletal-muscle. *Med Sci Sport Exer.* 1975; 7:185–198.
7. Nerem RM. Vascular Fluid-Mechanics, the Arterial-Wall, and Atherosclerosis. *J Biomech Eng.* 1992; 114:274–282. [PubMed: 1522720]
8. Carey BJ, Patra PK, Ci L, Silva GG, Ajayan PM. Observation of dynamic strain hardening in polymer nanocomposites. *ACS Nano.* 2011; 5:2715–2722. [PubMed: 21410237]
9. Mullins L. Softening of Rubber by Deformation. *Rubber Chem Technol.* 1969; 42:339–362.
10. Diani J, Fayolle B, Gilormini P. A review on the Mullins effect. *Eur Polym J.* 2009; 45:601–612.
11. Hammerschmidt K, Finkelmann H. Stress-optical and thermomechanical measurements on liquid-crystalline elastomers. *Makromol Chem.* 1989; 190:1089–1101.
12. Kundler I, Finkelmann H. Strain-induced director reorientation in nematic liquid single crystal elastomers. *Macromol Rapid Commun.* 1995; 16:679–686.
13. Mitchell GR, Davis FJ, Guo W. Strain-induced transitions in liquid-crystal elastomers. *Phys Rev Lett.* 1993; 71:2947–2950. [PubMed: 10054819]
14. Schaezle J, Kaufhold W, Finkelmann H. Nematic elastomers: the influence of external mechanical stress on the liquid-crystalline phase behavior. *Makromol Chem.* 1989; 190:3269–3284.
15. Urayama K, Mashita R, Kobayashi I, Takigawa T. Stretching-induced director rotation in thin films of liquid crystal elastomers with homeotropic alignment. *Macromolecules.* 2007; 40:7665–7670.
16. Urayama K, Kohmon E, Kojima M, Takigawa T. Polydomain-monodomain transition of randomly disordered nematic elastomers with different cross-linking histories. *Macromolecules.* 2009; 42:4084–4089.
17. Warner, M.; Terentjev, EM. *Liquid Crystal Elastomers*. Oxford University Press; Oxford: 2003.

18. Finkelmann H, Kock HJ, Rehage G. Investigations on liquid-crystalline polysiloxanes. 3 liquid-crystalline elastomers - a new type of liquid-crystalline material. *Makromol Chem Rapid Commun.* 1981; 2:317–322.
19. Kupfer J, Finkelmann H. Nematic liquid single-crystal elastomers. *Makromol Chem Rapid Commun.* 1991; 12:717–726.
20. Finkelmann H, Greve A, Warner M. The elastic anisotropy of nematic elastomers. *Eur Phys J E Soft Matter.* 2001; 5:281–293.
21. Warner M, Terentjev EM. Nematic elastomers A new state of matter? *Prog Polym Sci.* 1996; 21:853–891.
22. Mitchell GR, Davis FJ, Ashman A. Structural studies of side-chain liquid crystal polymers and elastomers. *Polymer.* 1987; 28:639–647.
23. Bassett, DC. *Developments in Crystalline Polymers-2.* Elsevier Applied Science; London: 1988.
24. Dorfmann A, Ogden RW. A constitutive model for the Mullins effect with permanent set in particle-reinforced rubber. *Int J Solids Struct.* 2004; 41:1855–1878.
25. Munoz MJ, et al. An experimental study of the mouse skin behaviour: Damage and inelastic aspects. *J Biomech.* 2008; 41:93–99. [PubMed: 17826784]
26. Dorfmann A, Trimmer BA, Woods WA. A constitutive model for muscle properties in a soft-bodied arthropod. *J R Soc Interface.* 2007; 4:257–269. [PubMed: 17251157]
27. Schmoller KM, Fernández P, Arevalo RC, Blair DL, Bausch AR. Cyclic hardening in bundled actin networks. *Nat Commun.* 2010; 1
28. Ali SA, Al-Muallem HA, Rahman SU, Saeed MT. Bis-isoxazolidines: A new class of corrosion inhibitors of mild steel in acidic media. *Corros Sci.* 2008; 50:3070–3077.
29. Clarke SM, Terentjev EM. Slow stress relaxation in randomly disordered nematic elastomers and gels. *Phys Rev Lett.* 1998; 81:4436–4439.
30. Schneider F, Fellner T, Wilde J, Wallrabe U. Mechanical properties of silicones for MEMS. *J Micromech Microeng.* 2008; 18:065008.

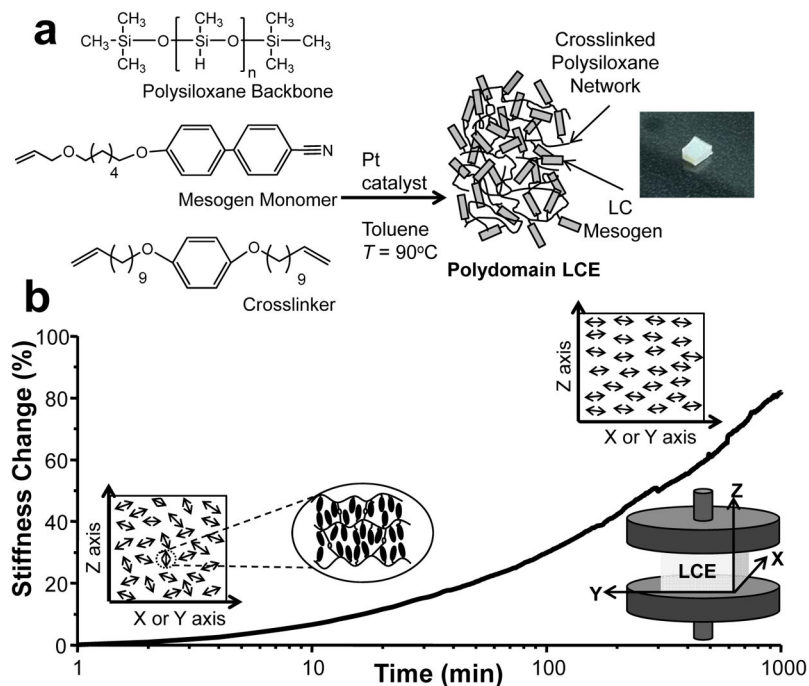


Figure 1. Synthesis and dynamic strain stiffening of polydomain LCEs

a, Schematic for the synthesis of a polydomain LCE. A representative LCE sample is shown on the right-hand side, and dynamic mechanical testing was carried out on LCEs with dimensions of 1.5 mm x 1.5 mm x 1 mm. **b**, Change in stiffness (%) versus time for a LCE (LCE90) under repetitive (dynamic) compression. The LCE is dynamically compressed between two flat plates at 5 Hz, 45 °C, a pre-load of 0.01N, and a 5 % strain amplitude using a DMA Q800. Schematics in the bottom-left and top-right show the alignment of nematic domains in LCEs subjected to repetitive compression. The inset in the bottom right shows schematic of experimental protocol employed for the dynamic compression of polydomain LCEs. The data shown are plotted on linear-log axes, and data on linear-linear axes is provided in the Supplementary Figure S5. A plot of the time-dependent strain applied to the sample during measurement is shown in Supplementary Figure S6.

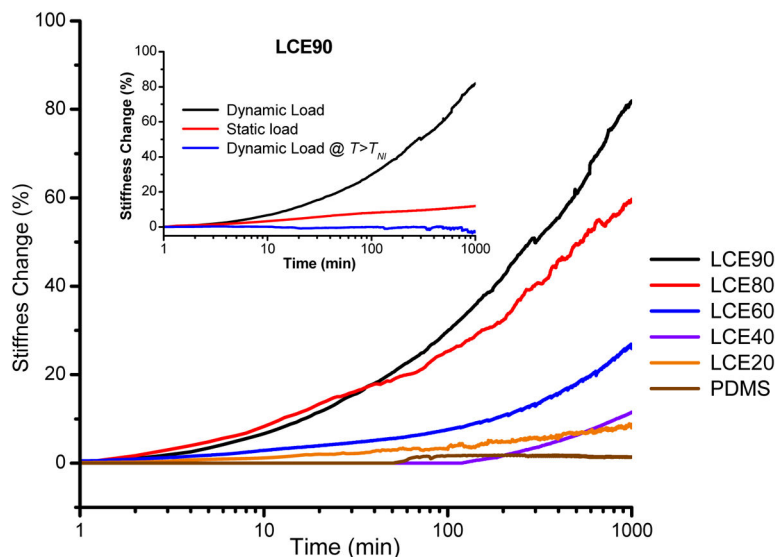


Figure 2. Dynamic strain stiffening in LCEs with varying mesogen content

Change in stiffness (%) versus time for a series of LCEs varying in mesogen content and PDMS under dynamic compressive strain. The data shown are plotted on linear-log axes, and data on linear-linear axes is provided in the Supplementary Figure S4. The extent of stiffening is correlated with LCE mesogen content. Measurements were carried out at 5 Hz, 45 °C and at 5% strain amplitude. The top inset compares dynamic strain stiffening in LCE90 under dynamic load, static load and dynamic load above T_{NI} (80 °C) and demonstrates that stiffening is only observed in the nematic phase under dynamic compression. For static load tests, samples were subjected to a compressive strain of 6%, both greater than the corresponding stress and strain values applied during dynamic loading.

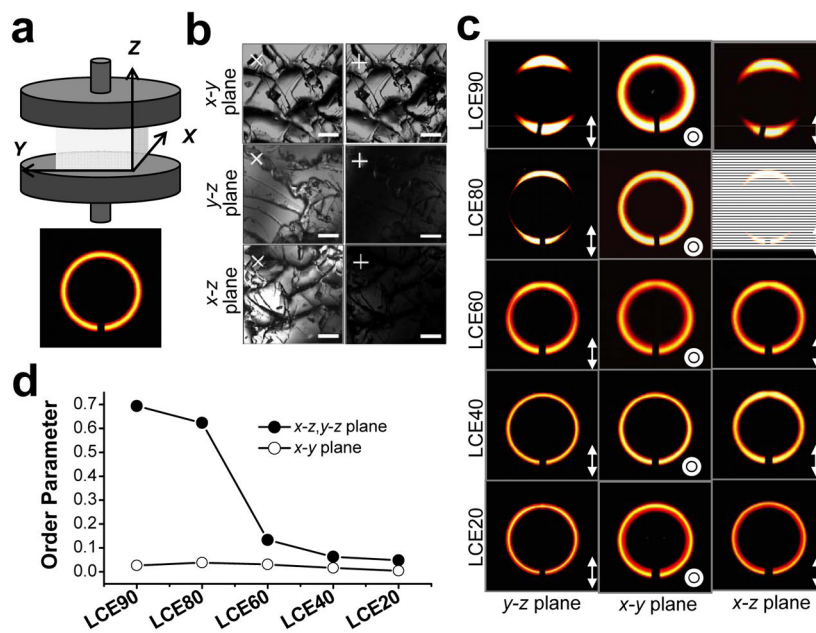


Figure 3. Microstructure analysis of LCEs after dynamic compression

a, Schematic of geometry during dynamic compression experiment and 2DWAXD pattern of unstressed, polydomain LCE90. All LCEs exhibit similar 2DWAXD patterns before dynamic compression. **b**, Polarizing optical microscopy images of dynamically stressed LCE90 along three different faces. Reduced light transmission through the x - z and y - z faces when crossed polarizers are oriented parallel to the compression direction (z -axis) indicates reorientation of the nematic director perpendicular to the z -axis. All scale bars represent 0.1 mm. **c**, 2D WAXD patterns of LCEs with varying mesogenic content subjected to compressive dynamic load (5 Hz, 5 % strain) for at least 16 hours. The patterns are shown for three independent LCE faces (x - z plane, x - y plane, and y - z plane), and the arrow on the bottom right hand side indicates the direction of compression. The anisotropic scattering pattern observed for the x - z and y - z planes indicates that the LCE nematic director rotates away from the z -axis (compressive direction) to lie primarily in the x - y plane, but the nematic director remains disordered in the x - y plane. **d**, Macroscopic alignment parameter S for dynamically stressed LCEs extracted from model fit of 2DWAXD pattern. The order parameter S is defined with respect to the x - y plane. The order parameters for the x - z and y - z planes is an average of the order parameters measured in each plane.

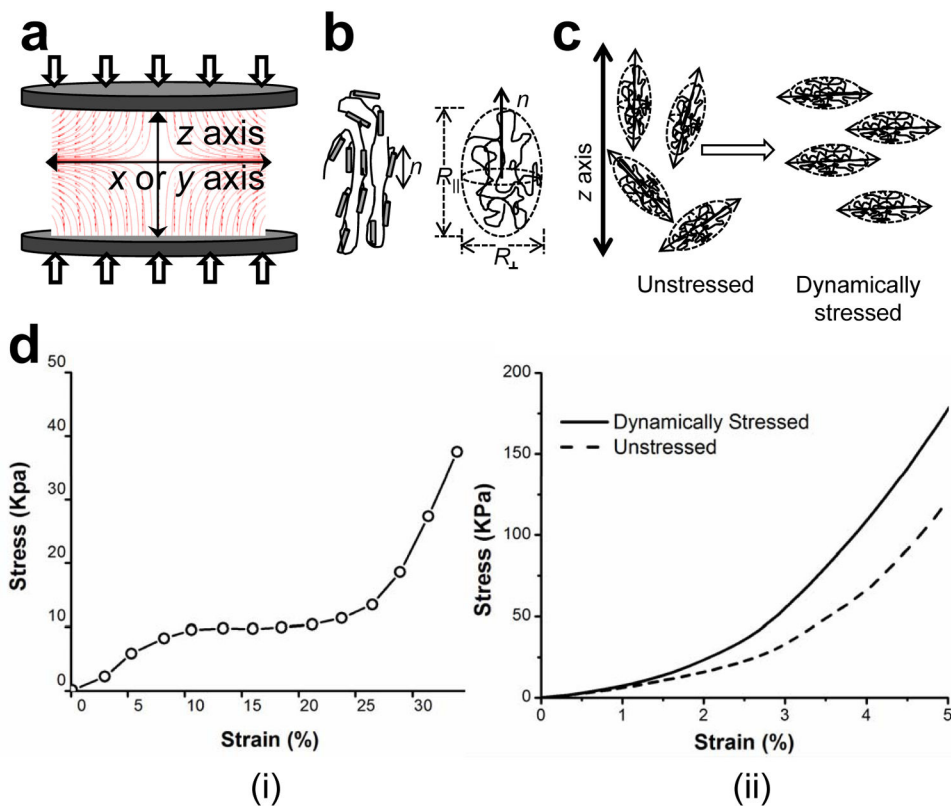


Figure 4. Reorientation of LC polymer chains under dynamic compression

a. Finite element modeling (FEM) simulation showing stress lines as a result of compression. FEM simulations were performed out using COMSOL Multiphysics 4.2 simulation package. **b.** Schematic depiction of a prolate LC polymer chain. Note that the mesogenic side-groups are oriented preferentially parallel to the polymer backbone. **c.** Reorientation of prolate LC polymer chains under compressive strain. **d.** Stress-Strain relationship of (i) polydomain LCE under uniaxial tension (data reproduced with permission from Clarke et al.²⁹) and (ii) polydomain LCE90 before and after dynamic compression. For LCE90 stress-strain profiles are recorded along the compression axis.

Table 1

Characteristics of LCEs and PDMS

Sample	Mesogen Content ^a (mole %)	Crosslinker Content ^a (mole %)	T_N ^b (°C)	Initial Stiffness ^c (N/m)	Final Stiffness ^d (N/m)	Change in Stiffness ^d (%)
LCE90	90	10	67	5308	10201	89
LCE80	80	20	55	5493	8960	63
LCE60	60	40	50	7521	10005	33
LCE40	40	40	N/A	6708	7358	14
LCE20	20	40	N/A	6471	7388	14
PDMS	NA	0.493 ^e	NA	4090	4145	1.4

^a relative to molar content of Si-H in PHMS^b measured by DSC; where no value is listed, no measurable T_N was found down to 0 °C^c measured at 5% strain^d measured at 5% strain after ~17 hours of continuous dynamic compression^e degree of crosslinking $\text{nm}^{-3}(30)$